Science Advances

AAAS

advances.sciencemag.org/cgi/content/full/3/9/e1700688/DC1

Supplementary Materials for

A customizable class of colloidal-quantum-dot spasers and plasmonic amplifiers

Stephan J. P. Kress, Jian Cui, Patrik Rohner, David K. Kim, Felipe V. Antolinez, Karl-Augustin Zaininger, Sriharsha V. Jayanti, Patrizia Richner, Kevin M. McPeak, Dimos Poulikakos, David J. Norris

Published 22 September 2017, *Sci. Adv.* **3**, e1700688 (2017)
DOI: 10.1126/sciadv.1700688

This PDF file includes:

Supplementary Materials

section S1. Computation of mode stability

To find stable plasmonic cavity geometries, we exploit the conditions derived for laser-cavity design via the matrix-transfer method. For symmetric cavities that have two mirrors of identical curvature, a single geometric parameter, $g = 1 - \frac{L}{R}$, determines the stability. Here, L is the inter-mirror spacing and R is the mirror curvature. The matrix-transfer method shows that a symmetric cavity supports stable, reproducing modes when $-1 < g < 1$. Throughout this work, we used a symmetric cavity with $g = 0.5$, or mirrors that have a radius-of-curvature R that is twice the inter-mirror spacing, $R = 2L$.

section S2. Beam waist calculation and ray tracing

To better understand the propagation and extent of the mode in our cavity, we performed beam-waist and ray-tracing calculations. Beam-waist calculations were computed assuming that the modes in our cavities are well-approximated by 2D-Gaussian modes. 2D ray-tracing between the reflectors was performed using a simple in-house MATLAB code (Fig. 2A in the main text).

section S3. Cavity design

The symmetric cavities in this work consist of two mirrors with an inter-mirror spacing of $L = 10$ μm. These mirrors have a concave, parabolic geometry with an apex-radius-of-curvature that is two times the inter-mirror-spacing ($R = 2L = 20$ μm). The reflector blocks were typically designed to be 400 to 600 nm in height (H) to enable high reflectivity of the incident plasmons. The blocks had a width, W (see Fig. 2A), of 2 μm to avoid any detrimental shadowing effects during silver evaporation.

section S4. Plasmonic Fabry-Perot calculation for cavities

The modes of our planar plasmonic cavities can be modeled as a lossy one-dimensional Fabry-Perot resonator,

$$\frac{I_{\text{res}}}{I_0} = \frac{1}{(1-r_{\text{cav}})^2 + 4r_{\text{cav}}\sin^2\left(\frac{\pi\nu}{\nu_{\text{cav}}}\right)}$$

where $\frac{I_{\text{res}}}{I_0}$ gives the intensity modulation with frequency, ν, induced by the presence of the reflectors. The spectrum (*i.e.* strength and spacing) of these modes depends on the round-trip loss factor for the electric field,

$$r_{\text{cav}} = Re^{-l_0/L_{\text{mode}}}$$

and the characteristic cavity frequency,

$$\nu_{\text{cav}} = \frac{c_0}{2n_{\text{mode}}l}$$

where *R* is the plasmon reflectivity (intensity) of the reflectors, c_0 is the speed of light in vacuum, and l_0 is the geometric size of the cavity. L_{mode} and n_{mode} are the propagation length and effective index of the mode considered.

To determine the effective cavity length, *l*, the geometric cavity length l_0 has to be corrected by the penetration depth into the silver, δ (obtained from the Fresnel equations) (Ref. 38),

$$l = l_0 + 2\delta$$

In particular, L_{mode} and n_{mode} are strongly dispersive (as expected for plasmons), whereas the penetration depth, δ , and reflection coefficient, *R*, are only weakly dependent on the frequency ν. Both L_{mode} and n_{mode} are also dependent on the quantum-dot-layer thickness, t_{QD}, and refractive index, n_{QD}, as well as the dielectric function of the silver films, $\varepsilon_{\text{Ag}}(\nu)$.

section S5. Calculation of propagating modes in silver/quantum dot/air stack

For this infinite three-layer system (silver/quantum-dot-layer/air), we numerically calculated values for the mode index, $n_{\mathrm{mode}}(n_{\mathrm{QD}}, t_{\mathrm{QD}}, \varepsilon_{\mathrm{Ag}}, \nu)$, and propagation length, $L_{\mathrm{mode}}(n_{\mathrm{QD}}, t_{\mathrm{QD}}, \varepsilon_{\mathrm{Ag}}, \nu)$, from analytical expressions as previously reported (Ref. 39). This analysis allows us to retrieve all modes (both photonic and plasmonic) propagating along the interface in our three-layer system. Once we solve for the complex wave-vectors, $k_{\mathrm{mode}}(n_{\mathrm{QD}}, t_{\mathrm{QD}}, \varepsilon_{\mathrm{Ag}}, \nu)$ for the propagating modes are determined and we obtain the effective index,

$$n_{\mathrm{mode}} = \Re\left(\frac{k_{\mathrm{mode}}}{k_0}\right)$$

and propagation length,

$$L_{\mathrm{mode}} = \frac{1}{\Im\left(2k_{\mathrm{mode}}\right)}$$

of the modes, which are functions (see figs. S1 and S2). For the plasmonic mode in an infinitely thick quantum-dot layer, simple expressions for the effective refractive index,

$$n_{\mathrm{SPP}}(n_{\mathrm{QD}}, \varepsilon_{\mathrm{Ag}}, \nu) = \Re\left(\sqrt{\frac{n^2{}_{\mathrm{QD}}\varepsilon_{\mathrm{Ag}}(\nu)}{n^2{}_{\mathrm{QD}} + \varepsilon_{\mathrm{Ag}}(\nu)}}\right)$$

and propagation length of the plasmonic mode,

$$L_{\mathrm{SPP}}(n_{\mathrm{QD}}, \varepsilon_{\mathrm{Ag}}, \nu) = \frac{c_0}{4\pi\nu}\Im\left(\sqrt{\frac{n^2{}_{\mathrm{QD}} + \varepsilon_{\mathrm{Ag}}(\nu)}{n^2{}_{\mathrm{QD}}\varepsilon_{\mathrm{Ag}}(\nu)}}\right)$$

can be found.

section S6. Optical characterization: Lifetime measurements

Time-resolved measurements were performed on the same microscope setup as described in the Materials and Methods Section. The pump laser was adjusted to 100 kHz for these measurements with power reduced to <1 nJ/cm^2. The emission was focused onto an avalanche photodiode

(Picoquant, MPD-SPAD) carefully placed at the image plane of a different exit port of the same spectrometer. This allowed us to spatially resolve the emission from the sample by moving the sample position using a piezo nanopositioning system (Mad City Labs, Nano-LPS300). A time-correlated single-photon-counting module (Picoquant, PicoHarp 300) was used to acquire time-resolved data. The time delay histograms were binned to 64 ps bin-widths and fit to a biexponential curve for the first 50 ns of the decay. These data were scaled such that the fit was normalized at $t = 0$ (fig. S4). Different measurements were compared at the $1/e$ value of the decay. The emission was collected from photoluminescence of quantum dots printed on fused silica, quantum dots printed on flat Ag, quantum dots printed into one of our cavities, and from plasmon scattering from the outer edge of the block reflector of the same cavity.

section S7. Spasing thresholds

We have observed spasing thresholds as low as 100 $\mu J/cm^2$ in our devices. As mentioned in the main text, this is somewhat surprising given that the best quantum-dot lasers, which should have lower losses, exhibit comparable values. The decreased thresholds may be attributed to Purcell enhancement of the quantum-dot emission rate, high coupling of this emission to the cavity mode, and high modal overlap. Time-resolved measurements suggest that the Purcell enhancement in our devices could be as high as ~2 (fig. S4). However, this estimate does not account for the effect of possible quenching of the emitter by the metal. The increase in output power above threshold (Fig. 3c), which, according to traditional laser rate equations (Ref. 17), scales inversely with the effective coupling factor β, indicates a relatively high effective value of ~0.06. Finally, the overlap between the plasmonic TM0 and the quantum-dot layer is very high (see fig. S1). These factors contribute to lower spasing thresholds as propagating plasmons can be more efficiently generated and stimulated.

section S8. Modal gain, plasmonic loss, and quantum dot material gain

A mode is amplified when the gain provided by the gain medium exceeds loss. The modal gain, g_{mode}, is given by the expression,

$$g_{\text{mode}} = \Gamma \cdot g_{QD} - \alpha_{\text{mode}}$$

Here, losses in the mode are included in α_{mode}, the modal loss coefficient (loss per unit length). The total gain is given by $\Gamma \cdot g_{QD}$, where g_{QD}, is the material gain provided by the quantum-dot layer, and the modal overlap factor Γ quantifies the spatial overlap of the mode and the gain medium. The modal overlap factor for the surface-plasmon-polariton mode is close to unity, $\Gamma \sim 1$, due to the strong confinement (fig. S1). This is also evident from the high effective index of the mode (fig. S2). Since reflection losses are negligible compared to propagation losses (computed from the measured permittivity for our silver obtained from ellipsometry), the latter determine the modal losses and we calculate a loss of $\alpha_{\text{mode}} = 810\ \text{cm}^{-1}$. This is close to values reported (Ref. 40) for photonic devices with quantum dots synthesized using a similar recipe ($g_{\text{QD}} = 750\ \text{cm}^{-1}$). However, for our system, we measured the modal gain on the tapered amplifier (Fig. 4 of the main text) to be $g_{\text{mode}} = 500\ \text{cm}^{-1}$ (fig. S5), which implies a higher material gain from the quantum dots ($g_{\text{QD}} = 1310\ \text{cm}^{-1}$). This high material gain may be due to enhancements in the Purcell factor (up to ~2) and β-coupling factor in our plasmonic device compared to the photonic case as discussed in Section S7 above.

section S9. Estimation of spasing threshold

We estimate the spasing threshold using the approach of Ref. 34. Using a 10-level coupled-rate-equation model, Chua *et al.* derive an analytical expression for the lasing threshold. They initially derive an expression for continuous-wave excitation and then adapt this to pulsed excitation:

$$U_{\text{pulse}}^{\text{thr}} \approx \frac{hf_{\text{p}}\tau_{\text{pulse}}}{\eta^{S_0S_1}} \times \frac{(F_{\text{p}}/\tau_{\text{spont}} + 1/\tau_{21})/\tau_{\text{loss}}^{'}}{F_{\text{p}}\beta V\Gamma_{\text{s}}/\tau_{\text{spont}} - 1/\left(N_{\text{tot}}^{\text{den}}\tau_{\text{loss}}^{''}\right)} \times V$$

See Table S1 and Ref. 34 for the definitions of variables. In addition,

$$\frac{1}{\tau_{\text{loss}}^{'}} = \frac{1}{\tau_{\text{loss}}} + v_{\text{g}}\sigma_{\text{abs}}^{S_0S_1}\Gamma_{\text{s}}N_{\text{tot}}^{\text{den}}$$

and

$$\frac{1}{\tau_{\text{loss}}^{''}} = \frac{1}{\tau_{\text{loss}}} + v_{\text{g}}\sigma_{\text{abs}}^{T_1T_2}\Gamma_{\text{s}}N_{\text{tot}}^{\text{den}}$$

with $Q_{\text{tot}} = 2\pi f_1\tau_{\text{loss}}$.

We inputted the parameters in Table S1 into the threshold equation. Despite the difference in photophysics between quantum dots and organic dyes, the calculation gives a pump threshold of 70 μJ/cm^2, in excellent agreement with our measured value of 100 μJ/cm^2. As mentioned in Ref. 34, this quasi-steady-state approximation tends to slightly underestimate the lasing threshold, but is still useful for understanding the system.

table S1. Parameters for threshold calculation.

Parameter	Value	Notes
Pump wavelength (f_p)	450 nm	Convert to Hz
Spasing wavelength (f_1)	633 nm	Convert to Hz
Pulse length (τ_{pulse})	340 fs	
Spasing quality factor (Q_{tot})	1000	For τ_{loss}
Spontaneous emission lifetime (τ_{spont})	10 ns	
Spontaneous emission enhancement (F_p)	1.7	
Non-radiative relaxation time (τ_{21})	1 ps	
Excitation Volume (V)	3.63×10^{-16} m^3	Pump spot size of 68 μm over an effective 100 nm QD layer
Emitter density (N_{tot}^{den})	6.08×10^{21}	Estimate number of 12nm diameter QDs in 10x2x0.1 μm stripe over V.
Spontaneous emission coupling factor (β)	0.06	
Fraction of energy in gain medium (Γ_s)	1	
Effective index of refraction (n_{eff})	1.7	For group velocity (v_g)
Absorption cross-section ($\sigma_{abs}^{S_0S_1}$)	10^{-13} cm^2	Estimate from literature
Absorption cross-section ($\sigma_{abs}^{T_1T_2}$)	0	Neglect triplet state absorption because pump pulse is so short
Fraction of pump power absorbed ($\eta^{S_0S_1}$)	9.24×10^{-5}	Consider fraction of power absorbed by QD stripe over a Gaussian with spot size 68 μm. Include 2 passes through QDs because of reflection from Ag surface.

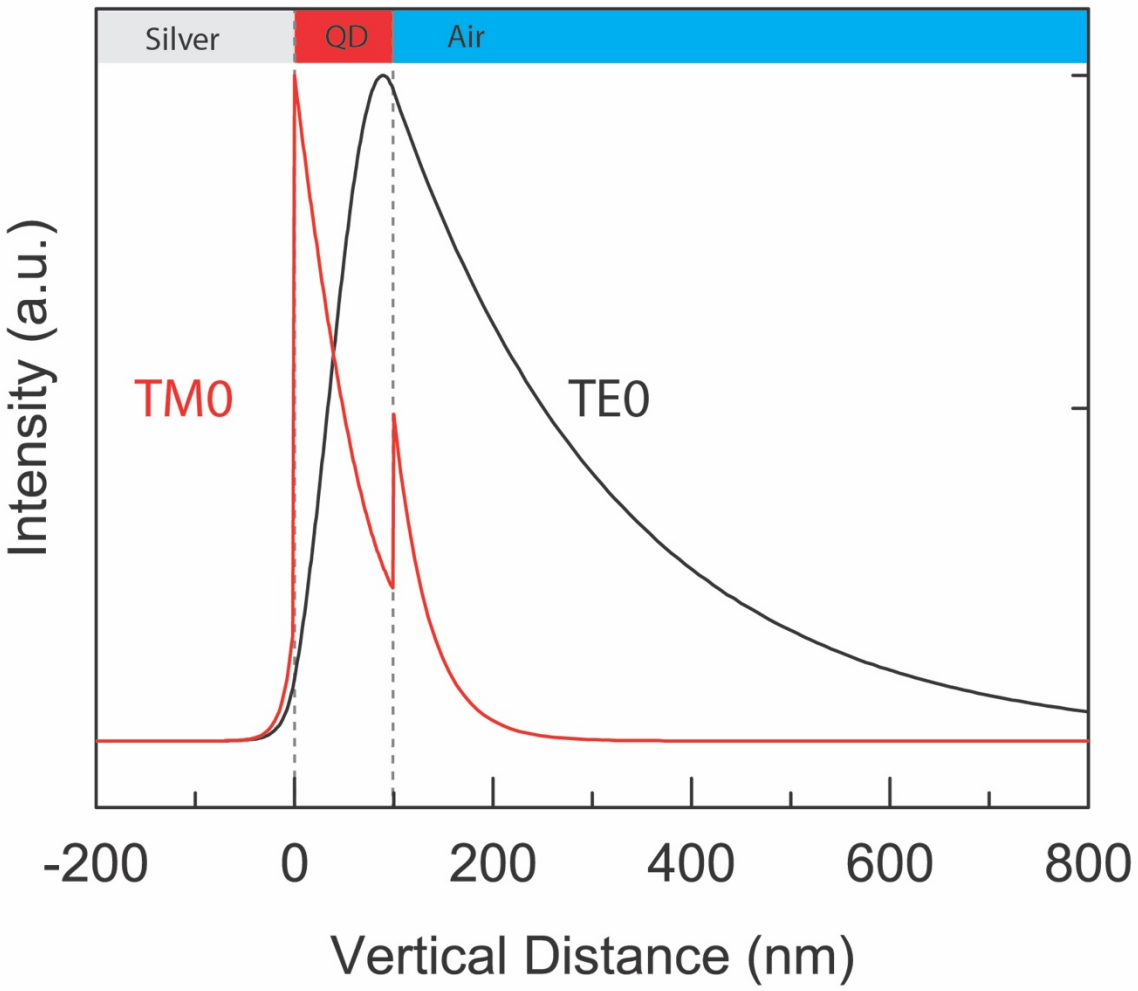

fig. S1. Calculated electric field profiles. The absolute value squared of the electric fields of the fundamental transverse magnetic (TM0) and fundamental transverse electric (TE0) modes calculated for a 100-nm-thick quantum-dot film on flat Ag. The plasmonic TM0 mode is confined closely to the Ag surface with high spatial overlap with the quantum dots. The photonic TE0 layer is extended far above the Ag surface and therefore has poor modal overlap with the quantum dots and decreased reflectivity from the block reflectors, which are 400 to 600 nm tall.

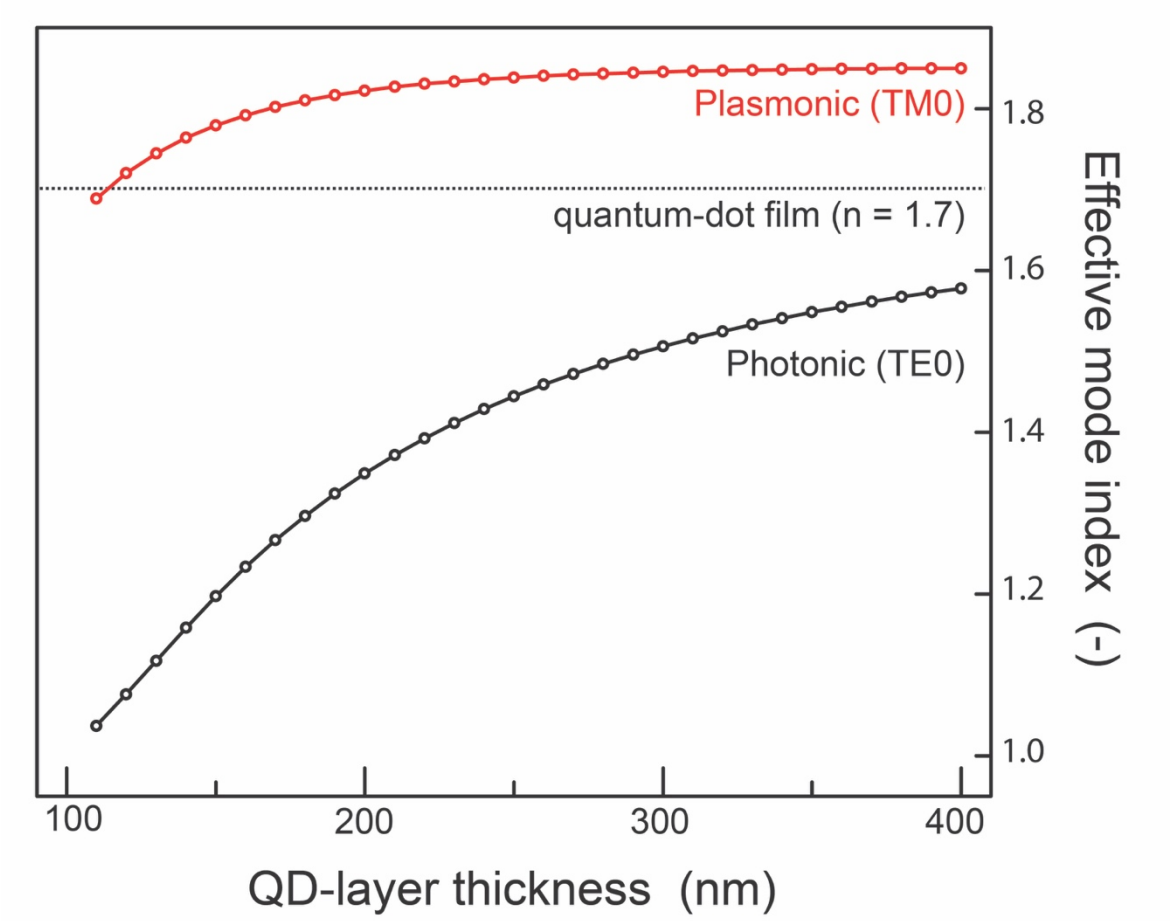

fig. S2. Calculated effective indices for plasmonic and photonic modes. The effective indices of refraction are plotted for the fundamental transverse electric (TE0) and transverse magnetic (TM0) modes at different thicknesses of the quantum-dot (QD) layer. The index of refraction, *n*, for a quantum-dot film is ~1.7, as indicated by the horizontal dotted line.

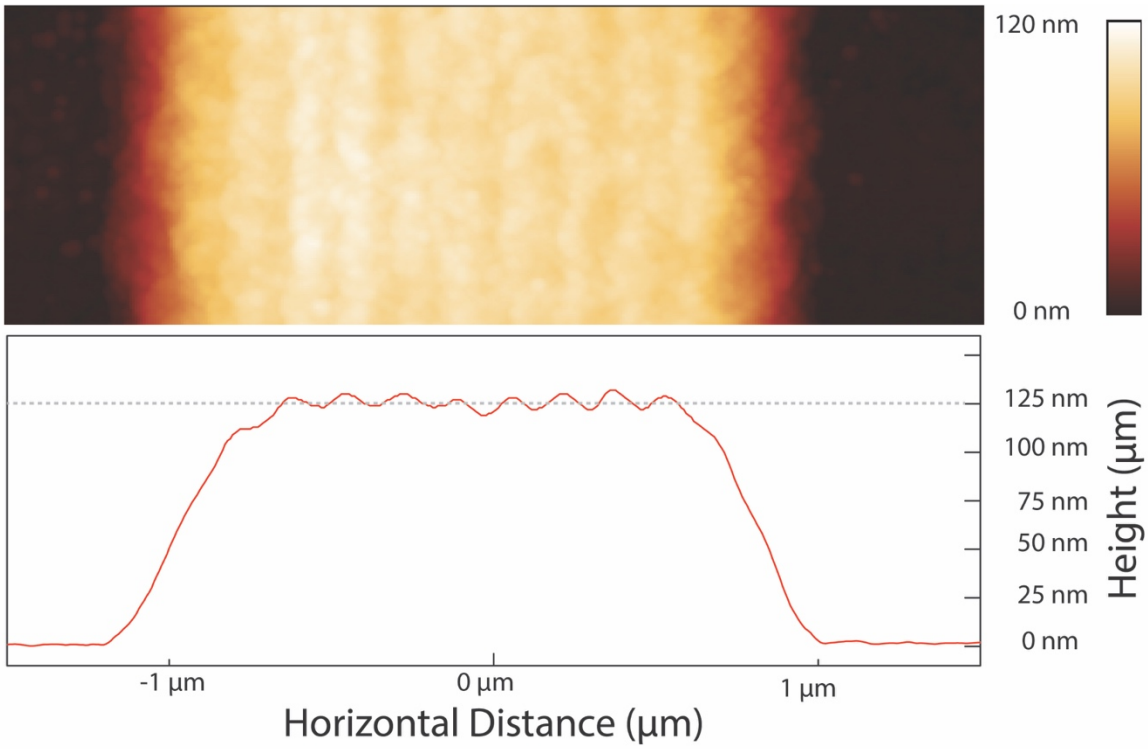

fig. S3. AFM topographic image of a printed quantum dot stripe. The topography of a typical colloidal quantum-dot stripe printed into a spaser cavity reveals that 9 overprints of quantum dots gives a height of ~125 nm.

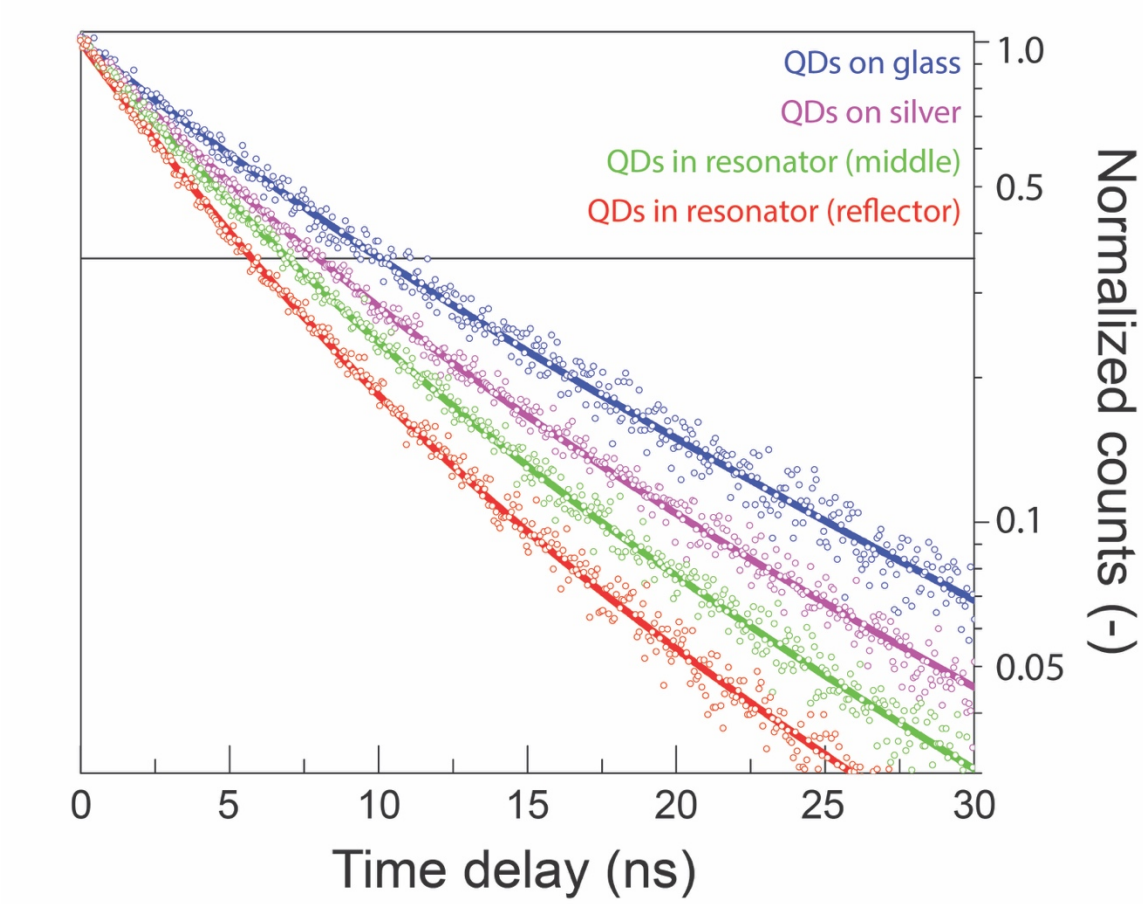

fig. S4. Lifetime measurements. The emission decay from quantum dots (QDs) and plasmons scattered from the outer edge of a block reflector measured using time-correlated single-photon counting. A comparison of the decay values at 1/*e* (horizontal line) between the quantum-dot photoluminescence on fused silica and the plasmon scattering from the outer reflector of the cavity indicates a Purcell enhancement of up to 2. See Sections S6 and S7.

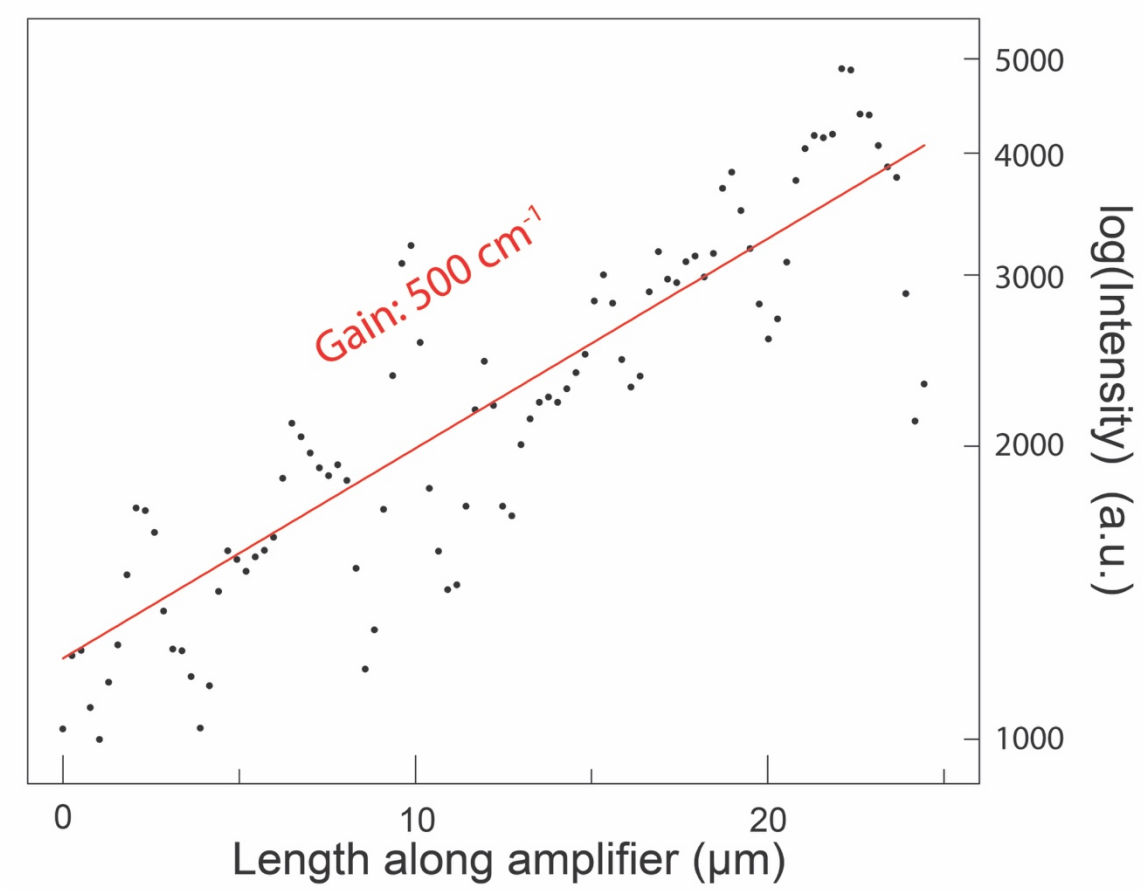

fig. S5. Measuring amplifier gain. An exponential fit to the increase in intensity along the length of the bottom edge of the elongated tip structure in Fig. 4 shows an amplification gain of 500 cm^{-1}.

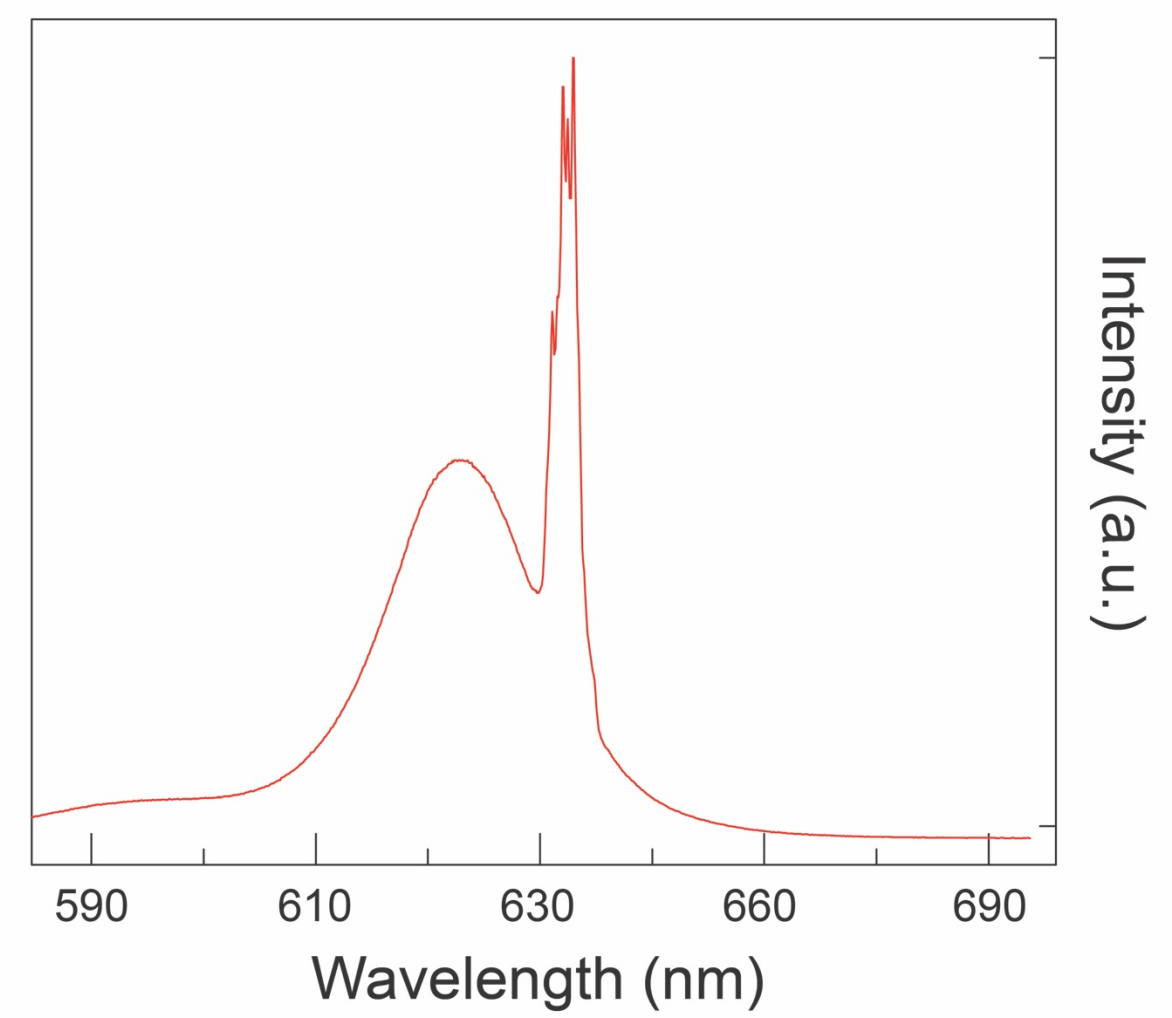

fig. S6. Amplified spontaneous emission at high excitation intensity. Excitation of the drop-cast quantum-dot film over a flat portion of the Ag chip shows amplified spontaneous emission at high excitation intensities. Though narrow spectral features can be resolved at the top of the amplified portion of the spectrum, these are unrelated to the spasing peaks observed within the plasmonic cavities.